View Article Online
View Journal

Dalton Transactions

An international journal of inorganic chemistry

Accepted Manuscript

This article can be cited before page numbers have been issued, to do this please use: Y. Zhou and Y. Zheng, *Dalton Trans.*, 2026, DOI: 10.1039/D5DT02950C.

ROYAL SOCIETY OF CHEMISTRY

rsc.li/dalton

View Article Online
DOI: 10.1039/D5DT02950C

Dalton Transactions

FRONTIER

Frontiers in circularly polarized photoluminescence and electroluminescence of chiral manganese(II) complexes

Received 00th January 20xx,
Accepted 00th January 20xx

DOI: 10.1039/x0xx00000x

Yong-Hui Zhou[1] and You-Xuan Zheng[2]*

Chiral luminescence materials and their application in biological sensors, mechanoluminescence, triboluminescence, radioluminescence, X-ray scintillation, and circularly polarized organic light emitting diodes have attracted wide attentions due to their circularly polarized luminescence properties. Among the chiral luminescence materials, the phosphorescent complexes with noble metals have been widely investigated, benefiting from the ability to harvest both singlet and triplet excitons in devices. However, phosphorescent manganese(II) complexes exhibit cost-effectiveness, good luminescent properties, and low toxicity, but the development of chiral Mn(II) complexes is slow. This review mainly focuses on the molecular design strategies, photophysical and chiroptical properties, and applications of chiral Mn(II) complexes in different aspects, while discusses the recent progress, challenges and outlook in this area.

Introduction

Due to the generation of circularly polarized luminescence (CPL), chiral materials have potential application in biological sensors, optical information storage, mechanoluminescence and triboluminescence, radioluminescence, X-ray scintillation, and circularly polarized (organic) light-emitting diode (CP-(O)LED), etc.[1-7] Among them, CP-(O)LED play an important role for and 3D display technology. To evaluate the CPL performances of chiral materials and CP-devices, there are two important parameters: dissymmetry factor (g_{lum} (g_{PL} and g_{EL})) and photoluminescence quantum yield (PLQY). Ideal chiral materials should have both high g_{PL} and PLQY values.

Experimentally, the g_{lum} factor is defined as $2 \times \Delta I/I = 2 \times (I_L - I_R)/ (I_L + I_R)$, where I_L and I_R represent the intensities of left- and right-handed CPL, respectively. Theoretically, the g_{lum} is defined as $4 \times |\mu_e| \times |\mu_m| \times \cos\theta_{e,m}/ (|\mu_e|^2 + |\mu_m|^2)$, where μ_e and μ_m denote the electric and magnetic transition dipole moments, and $\theta_{e,m}$ is the angle between $\vec{\mu}$ and $\vec{m}$, respectively. Therefore, the chiral materials with closed μ_e and μ_m values, and $\theta_{e,m}$ near 0° or 180° should show high g_{PL} factors. Furthermore, there is a trade-off relationship between the μ_e and μ_m, and efficient chiral materials often exhibit large μ_e values, but low μ_m data. Therefore, most chiral materials show low g_{lum} factors in theory, except for the magnetic transition permitted chiral lanthanide complexes.[8,9]

It is well known that in OLED, singlet (S_1) and triplet (T_1) excitons of the emitters are formed in a 1:3 ratio. Over the past decade, significant advancements have been made in chiral fluorescence, thermally activated delayed fluorescence (TADF), and phosphorescence materials.[10-19] For chiral fluorescent materials, only the exciton in S_1 state can be emitted and 75% of the electrically generated energy in T_1 state is dissipated, leading to a theoretical maximum internal quantum efficiency (IQE) of only 25%. Though TADF materials also emit fluorescence, they can achieve 100% IQE theoretically due to the fast upconversion from T_1 to S_1 through the reverse intersystem crossing. Furthermore, CP-OLEDs with chiral phosphorescent complexes, iridium(III) and platinum(II) complexes especially, can achieve 100% IQE via efficient spin-orbit coupling (SOC) effects induced by heavy metal atoms. However, the scarcity and high production cost of these precious metals contained materials pose significant challenges. Therefore, relative abundance metal based chiral phosphorescent complexes, such as manganese(II) complexes,[20-23] have garnered considerable interest, but the development of chiral Mn(II) complexes is slow.

This frontier provides a systematic overview of recent advancements in chiral Mn(II) complexes, including the molecular design strategy, photophysical and chiroptical properties, as well as their application in different areas.

Recent Progress of Chiral Mn(II) Complexes

Photophysical Mechanism for Mn(II) Complexes

Mn(II) ion has 5 single electrons, belonging to the $3d^5$ electron structure, resulting in 16 degenerate spin orbitals according to the Hund's rules. For the Mn(II) ion in the tetrahedral ligand field, the singlet orbital $6A_1$ is the ground state and the upper quadruple states ^4E, $^4A_1$ (G), and ^4E (D) have the same slope as the ground state $^6A_1$ on the Tanabe Sugano energy level diagram,[24-26] which explains the electronic transition from the ground state to the high-energy state. Therefore, as shown in Fig. 1(a), the absorption and emission transitions of Mn(II) mainly include the D and G terms. However, the photophysical properties of Mn(II) ions are constrained by their unique

View Article Online
DOI: 10.1039/D5DT02950C

excitation mechanism: the d-d transitions of the central metal (Laporte-forbidden) result in an extremely low molar extinction coefficient.[26,27] To overcome this limitation, researchers widely adopted triplet sensitization strategies, enabling efficient energy transfer from organic ligands with suitable energy level (Fig. 1(b)). The organic ligand acts as the "antenna" to absorb the energy to be excited to S_1 state. Through intersystem crossing, the exciton is transferred to T_1 state of the ligand. Then, the energy is transferred to the excited states of the Mn(II) ion, and the emission corresponding to the characteristic $^4T_1(G)\rightarrow{}^6A_1$ radiative transition is observed. This process must satisfy the following key conditions:[26-29] (1) Energy level alignment requirement. The triplet energy level (E_{T1}) of the ligand must be higher than the $^4A_1/^4A(G)$ excited state level of Mn(II) (23,256 $cm^{-1} \approx 2.88$ eV). The suitable energy level differences between E_{T1} and $E(^4A_1/^4A(G))$ are within 0.2–0.5 eV, which ensures sufficient driving force for energy transfer while preventing excessive energy gaps that would lead to non-radiative decay. (2) **Spatial coupling effect**. The distance between the ligand and Mn(II) must satisfy the requirements of the Dexter energy transfer mechanism (r < 10 Å). (3) **Orbital coupling strength**. The degree of orbital overlap between the ligand and Mn(II) center (characterized by the Hoffmann parameter κ) must reach above 10^{-3}, which can be achieved through conjugated ligand design to ensure effective electronic coupling.

The organic ligands in Mn(II) complexes primarily consist of electron-donating atoms such as nitrogen or phosphine oxides. The characteristic luminescence of Mn(II) complexes originates from the $^4T_1 \rightarrow {}^6A_1$ radiative transition, a process that is closely related to the crystal field strength (10Dq value).[23] According to crystal field theory, the luminescence of Mn(II) complexes can be systematically regulated through coordination number, ligand field strength, and spatial arrangement, enabling emission from green to near-infrared.

In tetrahedral coordination systems, the Mn(II) ion is typically surrounded by four atoms, forming isolated Mn(II)-ligand units. Under this coordination mode, the crystal field strength is relatively weak (10Dq ≈ 8000 cm^{-1}), and the Mn-Mn distance is large (>5 Å), effectively suppressing spin-spin coupling and resulting in emission wavelengths among 500-550 nm. In contrast, in octahedral coordination systems, forming linear chains within the crystal, the Mn(II) ion is surrounded by six atoms, and the distance between adjacent Mn(II) ions is significantly reduced (≈ 3.8 Å). This anisotropic structure produces a confinement effect, and in combination with the stronger crystal field strength (10Dq ≈ 12000 cm^{-1}), causes the redshifted emission wavelength to 580-700 nm. Furthermore, the Mn(II) ion also have three-, five-, seven-, and eight-coordination modes, which provide possibilities for the fine-tuning of luminescence properties of Mn(II) complexes. Furthermore, most Mn(II) complexes have long phosphorescence lifetimes of up to about 10 ms.

Over the past decade, Mn(II) complexes with diverse coordination types and luminescent colors, along with their applications in triboluminescence, mechanoluminescence, radioluminescence, thermal imaging, temperature sensors, X-ray radioluminescence and scintillation, information recording and security protection, LED and OLED, etc., have drawn significant attention. However, only few chiral Mn(II) examples have been reported and applied in CP-OLEDs with obvious CP electroluminescence (CPEL).

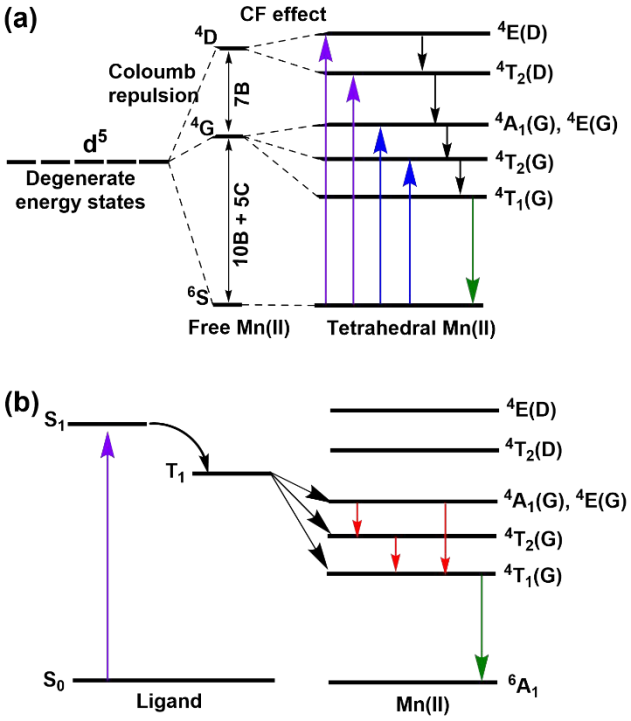

Fig. 1 Luminescence mechanism of tetrahedral Mn(II) ion (a) and complex (b).

Circularly Polarized Photoluminescence of Chiral Mn(II) Complexes

In 2020, D. Fu et al. reported perovskite enantiomorphic ferroelectrics, *R*/*S*-3-(fluoropyrrolidinium)$MnBr_3$ (*R*/*S*-1, Fig. 2(a)).[30] The red photoluminescence peaking at about 650 nm is produced by octahedrally coordinated Mn(II) ion. *R*/*S*-$MnBr_3$ show mirror-image CPL spectra compatible with the photoluminescence spectra associated with octahedral Mn(II) ions (Fig. 2(b)). The g_{PL} factors of the enantiomers are $\pm 6.1 \times 10^{-3}$ from 550 to 725 nm. The emergence of CPL activity for the two enantiomers dominated by the space configuration of the octahedral Mn(II) ions may be attributed to the influence of the introduction of chiral cations. This is the first molecular ferroelectric with CPL activity, holding great potential for the development of new optoelectronic devices.

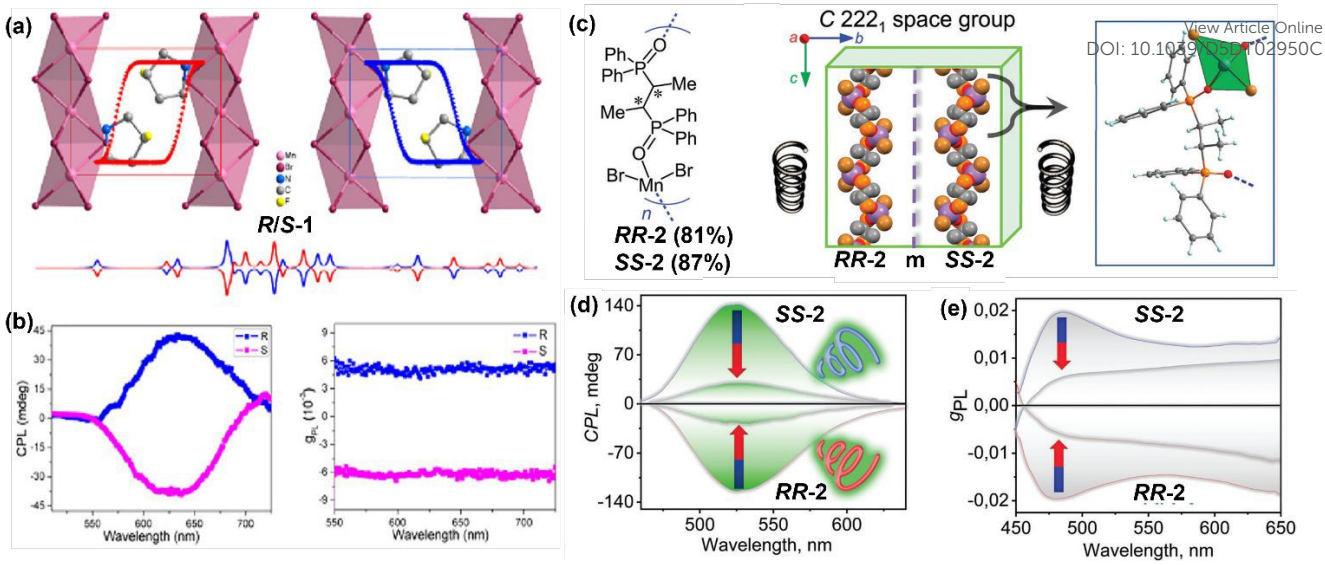

Fig. 2 (a) Packing views, (b) CPL spectra and g_{PL}- wavelength curves of *R*/*S*-1. Reproduced from ref. 30 with permission from American Chemical Society, copyright 2020. (c) Ligand and mirrored 1D helical chains of *RR*/*SS*-2 in the crystals (X-ray data). Right: X-ray structure of the repeating unit (The cyan, brown, orange, red, and gray spheres stand for Mn, Br, P, O, and C, respectively); (d) CPL and MCPL spectra and (e) g_{PL} - wavelength curves of *SS*-/*RR*-2: intensity attenuation upon a permanent magnetic field (1.6 T). Reproduced from ref. 31 with permission from Wiley-VCH, copyright 2023.

In 2023, A. V. Artem'ev et al. constructed a pair of chiral Mn(II) one-dimensional helical coordination polymers (*RR*/*SS*-2, Fig. 2(c)).[31] The enantiomers emit green emission peaking at 527 nm with a PLQY of 89% and an exceptionally high g_{PL} of 2.1 × 10^{-2}, while remaining ultrarobust toward humidity, temperature, and X-rays. Furthermore, this work revealed that an external magnetic field exerts a significant negative effect on the CPL of this Mn(II) material for the first time. Specifically, under a magnetic field of 1.6 T, the CPL signal was suppressed by a factor of 4.2 times (Fig. 2(d), (e)). In addition to these properties, the material also demonstrates an excellent linear response of emission intensity to temperature over the range of 77-298 K, along with bright mechanoluminescence and outstanding X-ray scintillation activity. Furthermore, the authors also fabricated the UV-pumped CP-LEDs with *RR*/*SS*-2 as phosphors with a large single crystal. The CP-LEDs exhibit strong green emission with only a single band peaking at 528 nm. Interestingly, an optical selectivity of output from the UV-pumped CP-LEDs is demonstrated. By passing through the configured polarizers, the generated light from the chiral emitters produces slightly different intensities. This interesting phenomenon can be explained by the generation of elliptically polarized light after the left circular polarized (LCP) and right circular polarized (RCP) light emitted from *SS*-2 and *RR*-2. More LCP light can pass through the left polarizer, and more RCP light goes through the right polarizer, and a slightly higher intensity of light appears for the corresponding chiral emitters when the direction of the linear polarizer is consistent with the long axis of the elliptically polarized light. This phenomenon was also appeared in their another work by combing luminogenic $[MnBr_4]^{2-}$ anions with *R*/*S*-[MBA-Me_3]$^+$ cations in a single ionic structure (MBA = *R*/*S*-*α*-methylbenzylamine). The obtained *R*/*S*-[MBA-Me_3]$MnBr_4$ (*R*/*S*-3) hybrids showed a near-unity PLQY and a high g_{lum} value of 4.5 × 10^{-3}, and the corresponding UV-pumped CP-LEDs also show excellent optical selectivity.[32]

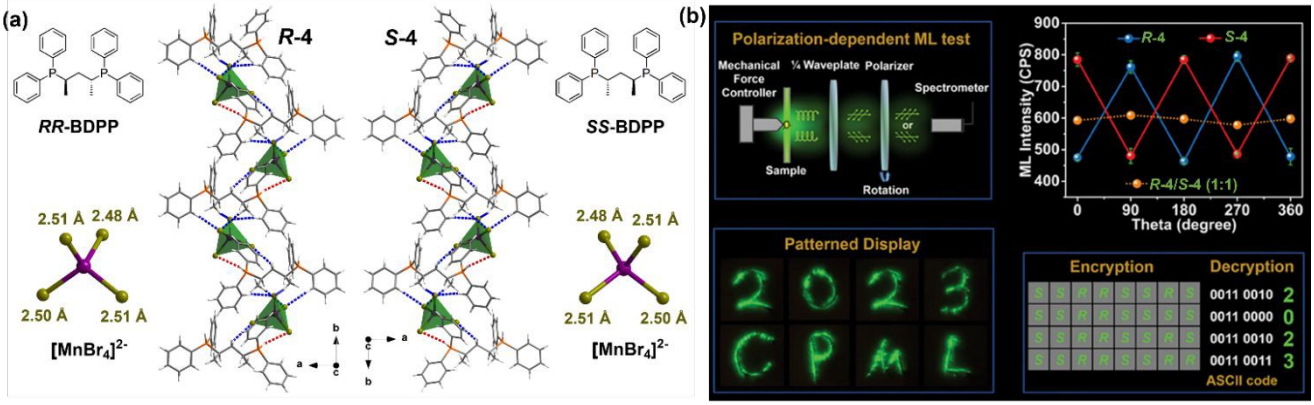

Fig. 3 (a) *RR*/*SS*-BDPP ligands and $[MnBr_4]^{2-}$ anion structures, and enantiomorphic crystal structures along the *b*-axis in *R*/*S*-4 (Br, Mn, P, C, and H atoms are colored in dark yellow, violet, orange, gray, and white, $MnBr_4$ units are displayed as green tetrahedra, respectively); (b) Schematic illustration of experimental setup to characterize CPML in *R*/*S*-4 and polarization-dependent ML emission intensities of chiral *R*-4, *S*-4, and a 1:1 racemic mixture of *R*/*S*-4 under 30 N force stimulation. Patterned display of ML emissions in *R*-4. Reproduced from ref. 33 with permission from Wiley-VCH, copyright 2024.

In 2024, Z. Quan et al. reported a pair of zero-dimensional (0D) Mn(II) bromide enantiomers, [H_2(2*R*,4*R*)-(+)/(2*S*,4*S*)-(-)-2,4-bis(diphenylphosphino)pentane]$MnBr_4$ (*R*/*S*-4, Fig. 3(a)).[33] By introducing the chiral bisphosphine ligands with rigid bulkiness and rich hydrogen bonds, they achieved the induction of non-centrosymmetric crystal structures. The resulting material exhibits near-unity PLQY and remarkable CPL performance, with g_{PL} values reaching ±2.0 × 10^{-3}. More importantly, this material demonstrates bright circularly polarized mechanoluminescence (CPML) under mechanical stimulation for the first time (Fig. 3(b)). It also shows an extremely high sensitivity to weak force stimuli (as low as 0.1 N), significantly outperforming traditional doped inorganic ML materials. Through structure-property relationship analysis, it was found that the excellent CPML performances of *R*/*S*-4 originate from their non-centrosymmetric $P2_1$ space group structure, abundant hydrogen-bonding network, and highly isolated luminescent centers. These features effectively promote the synergistic interaction between cleavage-induced charge separation and luminescent center excitation within the triboluminescence mechanism. Furthermore, this material exhibits a rare anti-thermal quenching effect across a broad temperature range (300-380 K), which is attributed to a thermally stimulated compensation process between trap states and the $^4T_1$ excited state of Mn(II). Based on their intriguing optical properties, these compounds as chiral force-responsive materials are demonstrated in multilevel confidential information encryption. This work provides a novel strategy and a theoretical foundation for the study of chiral hybrid metal halides in the fields of photonics information security, flexible electronic devices, and mechano-responsive optical functional materials.

Q. Zhao et al. reported a pair of axially chiral Mn(II) enantiomers, *R*/*S*-5 (ligand = 5,5'-bis(diphenylphosphine oxide)-4,4'-bi-1,3-benzodioxole), exhibiting five-coordinated structures.[34] Each Mn(II) ion is coordinated by four O atoms and one Br atom, forming a trigonal bipyramidal geometry (Fig. 4(a)). *R*/*S*-5 exhibit red emission centered at 636 nm with a PLQY around 70%. Simultaneously, *R*/*S*-5 demonstrate outstanding CPL property, featuring |g_{PL}| factors of up to 1.94 × 10^{-2} (Fig. 4(b)). By integrating *S*-5 with commercial phosphors, a white LED was fabricated with good performances. Furthermore, an exceptional scintillation performance was also observed, showcasing X-ray imaging with a spatial resolution of up to 11.9 lp mm^{-1}.

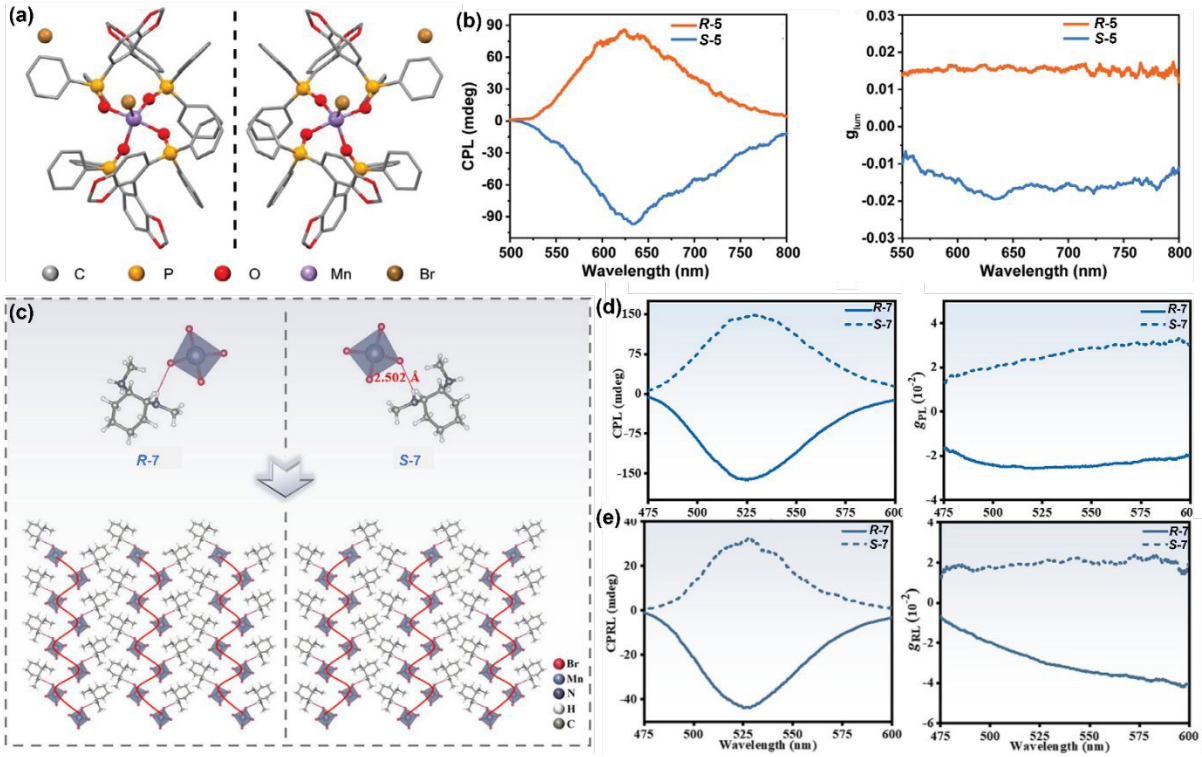

Fig. 4 (a) Crystal structures, (b) CPL spectra and g_{PL} - wavelength curves of *R*/*S*-5. Reproduced from ref. 34 with permission from Wiley-VCH, copyright 2024. (c) Crystal structures (Br: red, Mn: blue, N: bluish violet, H: white, C: grey); (d) CPL spectra, g_{PL} - wavelength curves and (e) CPRL spectra under X-ray illumination and g_{RL} -wavelength curves of *R*/*S*-7. Reproduced from ref. 35 with permission from Wiley-VCH, copyright 2025.

In 2025, Z. Chen et al. reported a pair of Mn(II) hybrid enantiomers, (1*R*/*S*,2*R*/*S*)-(*N*,*N*,*N*',*N*'-tetramethyl-1,2-cyclohexanediamine)$_2$$MnBr_4$·2$Br^-$ (*R*/*S*-6), which exhibit high PLQYs of around 94% and intense CPL spectra with |g_{PL}| factors of around 3.9 × 10^{-3}.[35] Furthermore, the enantiomers demonstrate strong scintillation performances with record-breaking light yields of 70061 and 68514 photons/MeV in chiral scintillators. This work pioneered quantitative evaluation of the circularly polarized radioluminescence (CPRL) of *R*/*S*-1, achieving g_{RL} factors of -2.04 × 10^{-3} and +2.55 × 10^{-3}. By incorporating hydrogen bonds into the structures to facilitate chiral transfer, Mn(II) hybrid enantiomers (1*R*/*S*,2*R*/*S*)-(*N*,*N*'-dimethyl-1,2-

View Article Online
DOI: 10.1039/D5DT02950C

cyclohexane-diamine)$MnBr_4$ (*R*/*S*-7, Fig. 4(c)) achieve the $|g_{PL}|$ values of around 2.5 × 10^{-2} (Fig. 4(d)), and their $|g_{RL}|$ values also increased to 2.96 × 10^{-2} (Fig. 4(e)). These values substantially surpass those of currently reported lead-free chiral scintillators, representing the state-of-the-art in chiroptical performance for this class of materials. This work manifests a new design strategy for advancing chiral scintillators and establishes a standard approach for evaluating CPRL properties.

Recently, X. Ren et al. reported a pair of chiral 0D Mn-Br hybrid enantiomers (*P*/*M*-8) through a crystallization-driven self-assembly strategy using entirely achiral molecular building blocks (Fig. 5).[36] In this system, the interaction between the non-centrosymmetric $[MnBr_4]^{2-}$ and the rotationally symmetric $[Pr\text{-}dabco]^{2+}$ (1-propyl-1,4-diazabicyclo-[2.2.2]octan-1-ium) cation, crystallizing in the chiral space group $P2_12_12_1$, achieved the induction and assembly of a chiral crystal structure. The *P*/*M*-8 single crystals exhibit excellent optical and chiroptical performances, with a PLQY of 68.8% and $|g_{PL}|$ values of up to 4.8 × 10^{-2}, respectively. Therefore, this combination achieves the record-high figure of merit of 4.2 × 10^{-2}. This study offers a robust strategy for the design and development of high-performance chiral luminescence materials utilizing achiral molecular architectures.

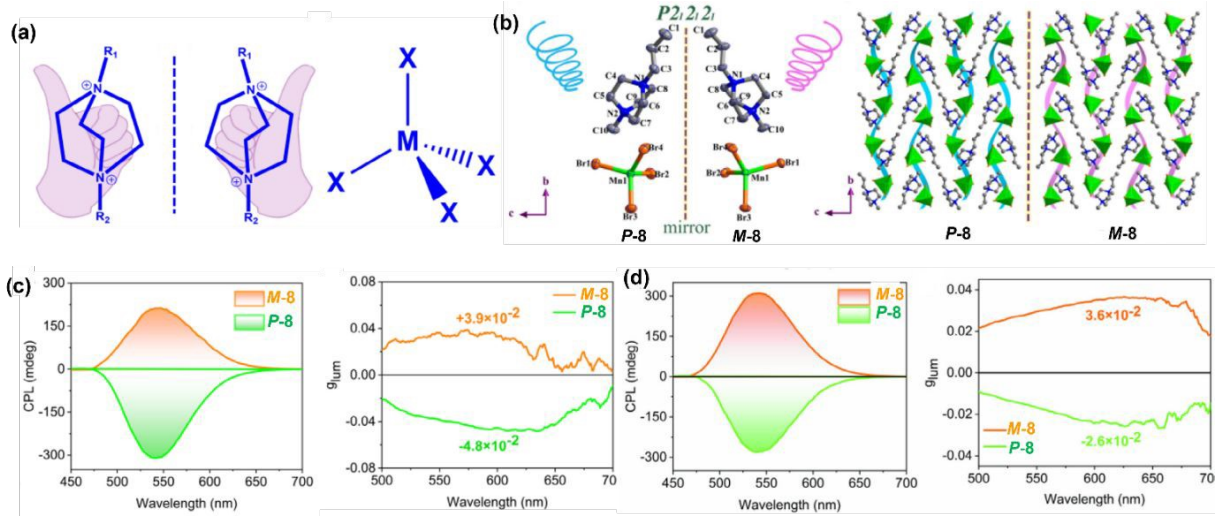

Fig. 5 (a) Molecular structures of rotational symmetric $[R_1,R_2\text{-DABCO}]^{2+}$ cation and tetrahedral $[MnX_4]^{2-}$ anion; (b) Asymmetric unit and enantiomorphic crystal structures of *P*/*M*-8 viewed along the *a* axis; (c) CPL spectra and g_{PL} - wavelength curves of *P*/*M*-8. (d) CPL spectra of CP-LEDs pumped by 360 nm UV and g_{EL} - wavelength curves of the CP-LEDs at a 5 V driving voltage. Reproduced from ref. 36 with permission from Wiley-VCH, copyright 2025.

Circularly Polarized Electroluminescence of Chiral Mn(II) Complexes

Because most chiral Mn(II) perovskites, ionic compounds and polymers can't be evaporated under vacuum, the CPEL was first obtained from CP-LED, fabricated by coating the chiral materials on the UV-LED chip. For example, X. Ren et al. fabricated the UV-LEDs based on *P*/*M*-8 enantiomers, which demonstrate outstanding performances, with a remarkable luminous brightness (74591 cd m^{-2}), and a high g_{EL} value of 3.2 × 10^{-2} (Fig. 5(d)).[36]

In 2024, W.-Y. Wong et al. proposed a strategy through steric hindrance-driven bond angle distortion for tuning the color of Mn(II) complexes, based on the dibenzofuran phosphine oxide skeleton.[37] By modulating the steric hindrance between the phosphine and the benzofuran units, as well as altering the O-Mn-O bond angles, five tetrahedral Mn(II) complexes achieve emission wavelengths within 498 - 548 nm. Interestingly, the single crystals of these achiral Mn(II) complexes exhibit CPL signals due to the symmetry breaking. Furthermore, the vacuum fabricated OLEDs achieve a record maximum external quantum efficiency (EQE_{max}) of 15.7%. But unfortunately, no CPEL signal was observed due to the unstable chiral structure.

In 2024, Z. Chen et al. reported a pair of Mn(II) enantiomers (*R*/*S*-9) based on the axially chiral ligands *R*/*S*-2,2'-bis(diphenylphosphinyl)-1,1'-binaphthyl, forming a distorted tetrahedral geometry (Fig. 6(a)).[38] The *R*/*S*-9 enantiomers display orange-red emission with peaks at 633/ 629 nm with PLQYs of 2.1%/4.0%, respectively. To elucidate the luminescence mechanism, they ruled out the possibilities of Mn-Mn coupling (lattice spacing of 8.6 Å) and self-trapped excitons. Calculations using the Tanabe-Sugano diagram yielded the Racah parameter of *B* = 835.6 cm^{-1} and the crystal field parameter of Dq = 1059.2 cm^{-1}, confirming the strong high crystal field environment created by the phosphine oxide ligands is the core driving force for the red emission. The enantiomers display $|g_{PL}|$ factors of 5.1 × 10^{-3} (Fig. 6(b)). Furthermore, corresponding solution-processed OLEDs show an EQE_{max} of 4.09% and $|g_{EL}|$ values of 8.5 × 10^{-3} (Fig. 6(c)).

View Article Online
DOI: 10.1039/D5DT02950C

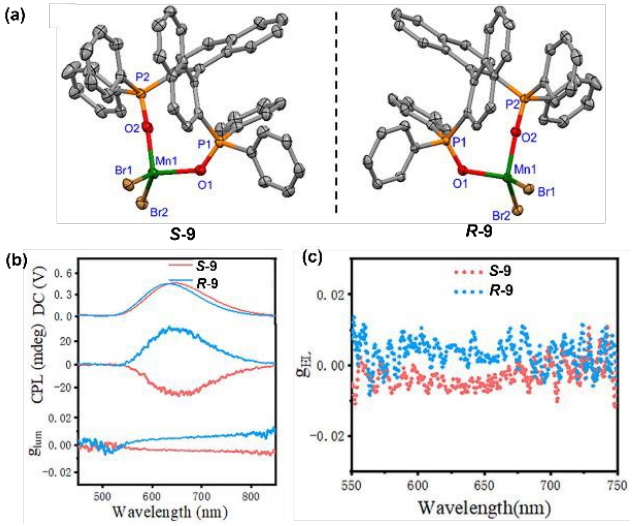

Fig. 6 (a) Single crystal structures and (b) CPL spectra and g_{PL} - wavelength curves of the *S*/*R*-9 enantiomers; (c) g_{EL} - wavelength curves of the doped devices based on *S*/*R*-9 enantiomers. Reproduced from ref. 38 with permission from Royal Society of Chemistry, copyright 2025.

Nearly at the same time, our group reported two pairs of chiral Mn(II) enantiomers (*R*/*S*-10 and *R*/*S*-11, Fig. 7(a)) based on phosphorus central chiral ligands, *tert*-butyl(6-(diphenylphosphoryl)dibenzo[*b*,*d*]furan-4-yl)(phenyl)phosphine oxide and *tert*-butyl(5-(diphenylphosphoryl)-9,9-dimethyl-9*H*-xanthen-4-yl)(phenyl)phosphine oxide.[39] The *R*/*S*-10 and *R*/*S*-11 enantiomers exhibit yellow-green emission peaking at 541 and 532 nm (Fig. 7(b)) with PLQYs of 87% and 77% in the solid state, respectively. Structural variations in the ligand backbones significantly impacted their emission properties. The rigid five-membered ring in DFPO led to denser packing and a higher radiative decay rate (2018 s^{-1}), compared to the more flexible six-membered XTDPO (1037 s^{-1}), thus resulting in a higher PLQY for complex 10. The $|g_{PL}|$ values of *R*/*S*-10 and *R*/*S*-11 enantiomers are 2.0 × 10^{-3} and 2.2 × 10^{-3} (Fig. 7(c)), respectively. The corresponding vacuum fabricated CP-OLEDs based on *R*/*S*-10 and *R*/*S*-11 deliver EQE_{max} values of 12.9% and 12.2% (Fig. 7(d)), with $|g_{EL}|$ factors of 1.5 × 10^{-3} and 1.8 × 10^{-3} (Fig. 7(e)), respectively. These findings validate the use of phosphorus-centered chiral ligands in constructing chiral Mn(II) complexes for efficient CP-OLEDs.

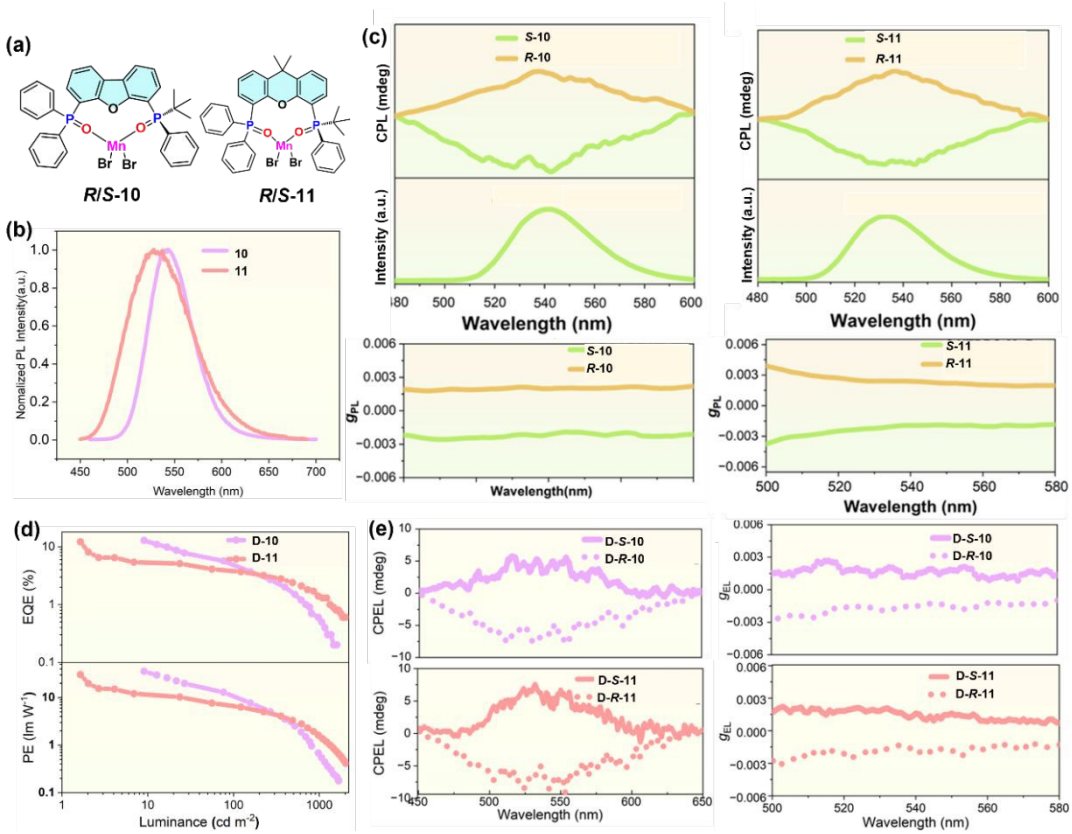

Fig. 7 (a) Molecular structures, (b) PL spectra, (c) CPL spectra and g_{PL} - wavelength curves of the *R*/*S*-10 and *R*/*S*-11 enantiomers; (d) External quantum efficiency–Luminance curves of D-10 and D-11 (OLEDs based on *rac*-10 and *rac*-11); (e) CPEL spectra and g_{EL} - wavelength curves of D-*R*/*S*-10 and D-*R*/*S*-11 (CP-OLEDs based on *R*/*S*-10 and *R*/*S*-11 enantiomers). Reproduced from ref. 39 with permission from Wiley-VCH, copyright 2025.

Recently, to further enhance both the g_{lum} value and device efficiency of the chiral Mn(II) complexes, [2.2]paracyclophane (pCp) was employed as a rigid planar chiral scaffold.[40] Chiral ligands were obtained by introducing phosphine oxide groups at the 4,13- and 4,12-positions of pCp, which were subsequently coordinated with $MnBr_2$ to afford two pairs of enantiomers: *R/S*-12 and *R/S*-13 (Fig. 8(a)). The rigid aromatic backbone and extended Mn-Mn distances of the Mn(II) complexes suppressed non-radiative losses, resulting in green emission with high PLQYs of up to 90%. Furthermore, the $|g_{PL}|$ values of *R/S*-12 and *R/S*-13 enantiomers reach 4.2 × 10^{-3} and 4.0 × 10^{-3} (Fig. 8(b)), respectively, which can be attributed to efficient chiral electronic transitions across the pCp framework. OLEDs based on the racemic complexes display notable EQE_{max} values of up to 16.0% (Fig. 8(d)), the highest for Mn(II) complexes-based OLEDs to date. In addition, the CP-OLEDs incorporating *R/S*-12 and *R/S*-13 enantiomers show high $|g_{EL}|$ values of 4.5 × 10^{-3} and 4.3 × 10^{-3} (Fig. 8(e)), approximately 2.5 times greater than those of their phosphorus central chiral analogues. This work reports the first planar chiral Mn(II) complexes and offers valuable design strategy for the development of high-performance chiral emitters for CP-OLEDs.

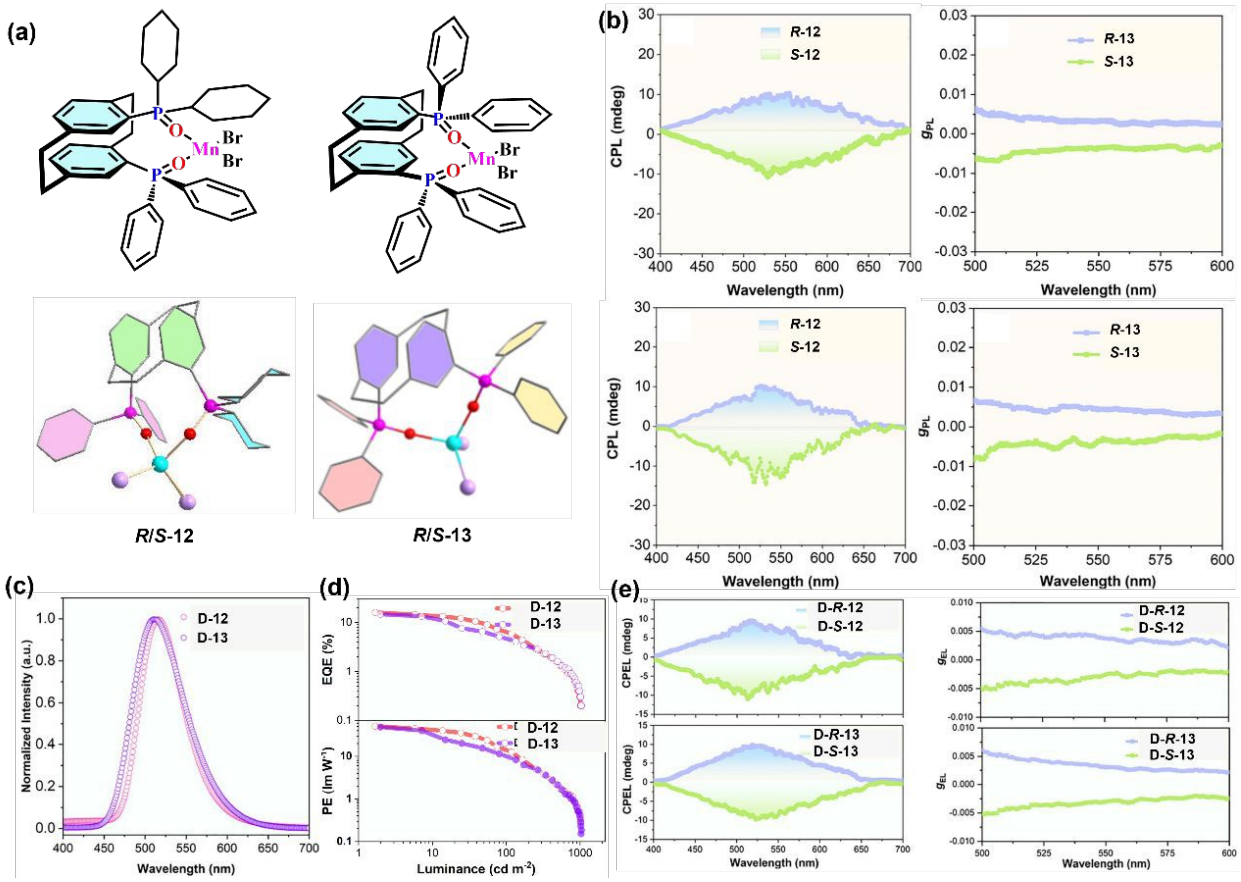

Fig. 8 (a) Molecular and single crystal structures, (b) CPL spectra and g_{PL} - wavelength curves of the *R/S*-12 and *R/S*-13 enantiomers; (c) EL spectra and (d) EQE–PE-Luminance curves of OLEDs based on racemic 12 and 13 complexes; (e) CPEL spectra and g_{EL} - wavelength curves of the CP-OLEDs based on *R/S*-12 and *R/S*-13 enantiomers. Reproduced from ref. 40 with permission from Science China Press and Springer, copyright 2025.

Conclusion and outlook

In conclusion, significant advancements of chiral Mn(II) complexes have been achieved in recent years, demonstrating their potential in multifunctional optoelectronic devices. However, there are only few isolated examples about the chiral organic complexes, chiral polymers, 0D Mn-Br hybrid enantiomers and perovskites have been applied in circularly polarized mechanoluminescence and triboluminescence, X-ray scintillation and imaging activity, radioluminescence and LED/OLED, etc. To date, only three examples of chiral Mn(II) complexes have been reported for CP-OLEDs in the literatures. But the design of novel chiral Mn(II) complexes that possess high luminescence efficiency and excellent chiroptical properties (high g_{lum} values especially), still remains significant challenge. At present, attention should be paid to the following aspects of research from our opinion:

(1) Molecular Design and Optical Tuning Mechanisms Need to be Clarified

Although different types of chiral Mn(II) frameworks have been investigated, a systematic theoretical guidance is still lacking. Especially, the maximum g_{lum} factors of chiral Mn(II) enantiomers are still at 10^{-2} level. Specifically, how to achieve predictable control over emission wavelength, emission

View Article Online
DOI: 10.1039/D5DT02950C

bandwidth, excited-state dynamics, and CPL property of chiral Mn(II) enantiomers through precise manipulation of ligand electronic structure, steric hindrance, and chiral environment requires further exploration. Current tuning methods still heavily rely on empirical accumulation and trial-and-error approaches, lacking universal design rules. This limits the expansion of chiral Mn(II) materials towards broader emission ranges and better CPL properties with high g_{PL} factors. Future efforts should integrate theoretical calculations to establish interpretable structure-property relationship models between ligands and chiroptical behaviours of chiral Mn(II) complexes, enabling more efficient spectral region control and innovative molecular design.

(2) Luminescence Lifetime Regulation Mechanisms Require Breakthroughs

As a first-row transition metal, Mn(II) exhibits weak SOC effects, and its luminescence typically manifests as phosphorescence from its triplet state with a long decay lifetime. Therefore, the chiral Mn(II) complexes thus exhibit emission lifetimes on the order of hundreds of microseconds, reflects the spin-forbidden nature of the emission process to some extent. But the long lifetimes of the chiral Mn(II) complexes also introduces a series of issues. In particular, it can easily induce exciton annihilation in OLEDs, such as triplet-triplet annihilation and triplet-polaron annihilation, leading to a severe efficiency roll-off in the devices at high brightness. Therefore, it is necessary to design suitable ligands to regulate chiral organic-inorganic hybrid and organic Mn(II) frameworks with short excited state lifetimes.

(3) CPEL Device Engineering Still Face Challenges

Although some chiral Mn(II) complexes have been applied in CP-OLEDs, their performances in key parameters such as brightness, efficiency, efficiency roll-off, and device stability still lags behind that of chiral TADF materials and Ir(III) complexes. Concurrently, most current devices employ non-doped structures or simple doping strategies, lacking in-depth control and systematic optimization of device physics mechanisms such as charge injection, transport, and recombination interfaces. Especially, most chiral Mn(II) hybrid materials cannot be evaporated and have poor solubility in most organic solvents. Follow-up research should strengthen the synergistic regulation of device structures, by developing better-matched functional layers and solution-processed methods.

(4) Multiple Types of Application Need to be Expanded

As discussed above, circularly polarized X-ray scintillation and imaging, radioluminescence, mechanoluminescence and triboluminescence, and CP-LEDs/CP-OLEDs have been explored based on chiral Mn(II) complexes. However, further exploration is needed for chiral Mn(II) complexes in other fields. Meanwhile, current research is still limited at the laboratory level, and there is still a significant gap from practical applications. Furthermore, due to stability factors, current research mainly focuses on divalent chiral Mn(II) materials, with emission wavelengths from green to near-infrared. This is also a research direction that can be attempted in chiral Mn(IV) hybridization or inorganic structures in the future, providing the regulation possibility in a larger spectral range.

Acknowledgements

This work was supported by National Natural Science Foundation of China (U23A20593).

Conflicts of interest

There are no conflicts to declare.

Notes and references

[1]*Jiangsu Key Laboratory of New Energy Devices & Interface Science, School of Chemistry and Materials Science, Nanjing University of Information Science & Technology, Nanjing 210044, P. R. China*
[2]*State Key Laboratory of Coordination Chemistry, School of Chemistry and Chemical Engineering, Nanjing University, Nanjing 210023, P. R. China. E-mail: yxzheng@nju.edu.cn*

References

1 J. R. Brandt, F. Salerno and M. J. Fuchter, *Nat. Rev. Chem.*, 2017, **1**, 0045.
2 Y. Sang, J. Han, T. Zhao, P. Duan and M. Liu, *Adv. Mater.*, 2020, **32**, 1900110.
3 L. Frédéric, A. Desmarchelier, L. Favereau and G. Pieters, *Adv. Funct. Mater.*, 2021, **31**, 2010281.
4 D.-W. Zhang, M. Li and C.-F. Chen, *Chem. Soc. Rev.*, 2020, **49**, 1331–1343.
5 Z.-L. Gong, X. Zhu, Z. Zhou, S.-W. Zhang, D. Yang, B. Zhao, Y.-P. Zhang, J. Deng, Y. Cheng, Y.-X. Zheng, S.-Q. Zang, H. Kuang, P. Duan, M. Yuan, C.-F. Chen, Y. S. Zhao, Y.-W. Zhong, B. Z. Tang and M. Liu, *Sci. China Chem.*, 2021, **64**, 2060-2104.
6 X. Yang, X. Gao, Y.-X. Zheng, H. Kuang, C.-F. Chen, M. Liu, P. Duan and Z. Tang, *CCS Chem.*, 2023, **5**, 2760-2789.
7 L. Yuan, Y.-P. Zhang and Y.-X. Zheng, *Sci. China Chem.*, 2024, **67**, 1097-1116.
8 F. Zinna, U. Giovanella and L. Di Bari, *Adv. Mater.*, 2015, **27**, 1791-1795.
9 F. Zinna, L. Arrico, T. Funaioli, L. Di Bari, M. Pasini, C. Bottab and U. Giovanella, *J. Mater. Chem. C,* 2022, **10**, 463-468.
10 X.-F. Luo, H.-B. Han, Z.-P. Yan, Z.-G. Wu, J. Su, J.-W. Zou, Z.-Q. Zhu, Y.-X. Zheng, J.-L. Zuo, *ACS Appl. Mater. Interfaces*, 2020, **12**, 23172-23180.
11 T.-Y. Li, Y.-M. Jing, X. Liu, Y. Zhao, L. Shi, Z. Tang, Y.-X. Zheng and J.-L. Zuo, *Sci. Rep.*, 2015, **5**, 14912.
12 M. Li, S.-H. Li, D. Zhang, M. Cai, L. Duan, M.-K. Fung and C.-F. Chen, *Angew. Chem. Int. Ed.*, 2018, **57**, 2889-2893.
13 Z. G. Wu, H. B. Han, Z. P. Yan, X. F. Luo, Y. Wang, Y. X. Zheng, J. L. Zuo and Y. Pan, *Adv. Mater.*, 2019, **31**, 1900524.
14 M. Li, Y.-F. Wang, D. Zhang, L. Duan and C.-F. Chen, *Angew. Chem. Int. Ed.*, 2020, **59**, 3500-3504.

View Article Online
DOI: 10.1039/D5DT02950C

15 S.-Y. Yang, Y.-K. Wang, C.-C. Peng, Z.-G. Wu, S. Yuan, Y.-J. Yu, H. Li, T.-T. Wang, H.-C. Li, Y.-X. Zheng, Z.-Q. Jiang and L.-S. Liao, *J. Am. Chem. Soc.*, 2020, **142**, 17756-17765.
16 W. Yang, N. Li, J. Miao, L. Zhan, S. Gong, Z. Huang and C. Yang, *CCS Chem.*, 2022, **4**, 3463-3471.
17 Q. Wang, L. Yuan, C. Qu, T. Huang, X. Song, Y. Xu, Y. X. Zheng and Y. Wang, *Adv. Mater.*, 2023, **35**, 2305125.
18 L. Yuan, Y.-F. Yang, Z.-P. Yan, J.-J. Hu, D. Mao, H.-X. N and, Y.-X Zheng, *Adv. Funct. Mater.*, 2024, **34**, 2403803.
19 X.-J. Liao, S. Xing, J.-J. Hu, X.-Z. Wang and Y.-X Zheng, *CCS Chem.*, 2025, **7**, 2419-2431.
20 L.-J. Xu, C.-Z. Sun, H. Xiao, Y. Wu and Z.-N. Chen, *Adv. Mater.*, 2017, **29**, 1605739.
21 Y. Qin, P. Tao, L. Gao, P. She, S. Liu, X. Li, F. Li, H. Wang, Q. Zhao, Y. Miao and W. Huang, *Adv. Optical Mater.*, 2018, **6**, 1801160.
22 P. Tao, S. J. Liu and W. Y. Wong, *Adv. Optical Mater.*, 2020, **8**, 2000985.
23 Y. Qin, P. She, X. Huang, W. Huang, Q. Zhao, *Coord. Chem. Rev.*, 2020, **416**, 213331.
24 C. Albert, G. David and M. Goodgame, *J. Am. Chem. Soc.*, 1962, **84**, 167-172.
25 M. T. Vala, C. J. Ballhausen, R. Dingle and S. L. Holt, *Mol. Phys.*, **1972**, *23*, 217.
26 Q. Zhou, L. Dolgov, A. M. Srivastava, L. Zhou, Z. Wang, J. Shi, M. D. Dramic'anin, M. G. Brikefg and M. Wu, *J. Mater. Chem. C*, 2018, **6**, 2652-2671.
27 V. Morad, I. Cherniukh, L. Pöttschacher, Y. Shynkarenko, S. Yakunin and M. V. Kovalenko, *Chem. Mater.*, 2019, **31**, 10161-10169.
28 J. Chen, Q. Zhang, F. Zheng, Z. Liu, S. Wang, A. Wu and G. Guo, *Dalton Trans.*, 2015, **44**, 3289-3294.
29 B. Su, M. S. Molokeev and Z. Xia, *J. Mater. Chem. C*, 2019, **7**, 11220-11226.
30 J.-X. Gao, W.-Y. Zhang, Z.-G. Wu, Y.-X. Zheng, D.-W. Fu, *J. Am. Chem. Soc.*, 2020, **142**, 4756−4761.
31 M. P. Davydova, L. Meng, M. I. Rakhmanova, Z. Jia, A. S. Berezin, I. Y. Bagryanskaya, Q. Lin, H. Meng and A. V. Artem'ev, *Adv. Mater.*, 2023, **35**, 2303611.
32 M. P. Davydova, L. Meng, M. I. Rakhmanova, I. Y. Bagryanskaya, V. S. Sulyaeva, H. Meng and A. V. Artem'ev, *Adv. Optical Mater.*, 2023, **11**, 2202811.
33 X. He, Y. Zheng, Z. Luo, Y. Wei, Y. Liu, C. Xie, C. Li, D. Peng and Z. Quan, *Adv. Mater.*, 2024, **36**, 2309906.
34 Z. Zhou, T. Jiang, Y. Yang, Y. Deng, M. Wang, Y. Ma, S. Liu and Q. Zhao, *Adv. Optical Mater.*, 2024, **12**, 2302185.
35 J.-Y. Yao, Q.-R. Ding, H. Zeng, J.-Y. Wang, C.-M. Shi, L.-J. Xu and Z.-N. Chen, *Angew. Chem. Int. Ed.*, 2025, **64**, e202502099.
36 L. Zhai, J. Yuan, J. Huang, X.-W. Pan, L. Wan, W. Ning and X.-M. Ren, *Angew. Chem. Int. Ed.*, 2025, **64**, e202425543.
37 P. She, Z. Zheng, Y. Qin, F. Li, X. Zheng, D. Zhang, Z. Xie, L. Duan and W.-Y. Wong, *Adv. Optical Mater.*, 2024, **12**, 2302132.
38 D.-H. Kong, Y. Wu, C.-M. Shi, H. Zeng, L.-J. Xu and Z.-N. Chen, *Chem. Sci.*, 2024, **15**, 16698-16704.
39 Z.-Z. Huo, Y. Wang, B. Yang, J.-Q. Liang, X.-F. Hong, Q. An, L. Yuan, H. Ma, J.-L. Zuo and Y.-X. Zheng, *Adv. Optical Mater.*, 2025, **13**, 2402684.
40 Z.-Z. Huo, X.-F. Hong, Y. Wang, X.-S. Zhong, X. Xiao, L. Yuan, Y.-H. Zhou and Y.-X. Zheng, *Sci. China Chem.*, 2025, **68**, 5673-5681.

View Article Online
DOI: 10.1039/D5DT02950C

Data Availability Statement

There is no data available in the frontier article.